Biophysical Journal Volume 109 September 2015 1190–1201

Article

Allosteric Dynamic Control of Binding

Fidan Sumbul,[1] Saliha Ece Acuner-Ozbabacan,[1] and Turkan Haliloglu[1,*]
[1]Department of Chemical Engineering and Polymer Research Center, Bogazici University, Istanbul, Turkey

ABSTRACT Proteins have a highly dynamic nature and there is a complex interrelation between their structural dynamics and binding behavior. By assuming various conformational ensembles, they perform both local and global fluctuations to interact with other proteins in a dynamic infrastructure adapted to functional motion. Here, we show that there is a significant association between allosteric mutations, which lead to high-binding-affinity changes, and the hinge positions of global modes, as revealed by a large-scale statistical analysis of data in the Structural Kinetic and Energetic Database of Mutant Protein Interactions (SKEMPI). We further examined the mechanism of allosteric dynamics by conducting studies on human growth hormone (hGH) and pyrin domain (PYD), and the results show how mutations at the hinge regions could allosterically affect the binding-site dynamics or induce alternative binding modes by modifying the ensemble of accessible conformations. The long-range dissemination of perturbations in local chemistry or physical interactions through an impact on global dynamics can restore the allosteric dynamics. Our findings suggest a mechanism for the coupling of structural dynamics to the modulation of protein interactions, which remains a critical phenomenon in understanding the effect of mutations that lead to functional changes in proteins.

INTRODUCTION

Proteins are dynamic entities under constant thermal motion. This arises from bonded and nonbonded interatomic interactions (hard to soft degrees of freedom) within the energy landscape, through physical principles of force and energetics. From local interactions to global motion, the local behavior from first principles leads to a behavior that is hierarchically at a higher level, allowing a more sophisticated picture of the dynamics that is utilized for a protein's function. The dynamics at this level is fairly well described by the intrinsic soft elastic modes of motion (1), where the hinges are the key components of the dynamic infrastructure for the collective behavior. Chemical or physical perturbations at hinge regions may lead to changes in the protein's structural functionality. These may appear in various forms, such as changes in stability and/or binding behavior, and a change in the dynamics with or without a main conformational change. Although various network models have been developed to explain the dissemination of a local perturbation in the structure (2), the mechanisms underlying local to global changes still remain elusive.

Allosteric regulation has recently been examined as a means of controlling protein function. Allostery was shown to be a fundamental property of both multiple- and single-domain proteins (3). It may be triggered by another protein, small-molecule or chemical modifications that can lead to opening/closing of the active site, or modifications of the physicochemical properties of functional sites through conformational changes and/or dynamics (4). Indeed, allosteric effects may involve a combination of these mechanisms, and our current understanding is that all of them may occur through a population shift in the protein's conformational ensemble (5,6). Dynamically fluctuating conformational ensembles and a shift in the ensemble of distributions provide an aspect of allosteric events with local physical/chemical changes (7). A linker/hinge with an inherent conformational preference can bias the sampling of conformational space that may result in an allosteric event in one domain or in a subdomain (3). Backbone or side-chain movements accompanied by some changes in local interactions may result in a global rearrangement of accessible conformational states.

A hinge bending motion may underlie differential specificity toward ligands for the proteins of a family, as suggested in an early study (8). Interestingly, a comparison of the protein dynamics of a hyperthermophilic and a mesophilic adenylate kinase showed that the physical origin of catalytically important collective domain motions relies on local hinge motions, and hinge fluctuations are encoded by differences in the amino acid sequence (9). A potent inhibitor that binds away from the catalytic site of an enzyme was observed to disrupt substrate binding and catalysis by preventing a hinge-like motion, and thus reverse a substrate-associated conformational change (10). Likewise, other studies have shown that changes in an allosteric network can affect the binding affinities in PDZ domains (11), and highlighted the importance of structural flexibility

Submitted March 4, 2015, and accepted for publication August 13, 2015.
*Correspondence: halilogt@boun.edu.tr
Fidan Sumbul and Saliha Ece Acuner-Ozbabacan contributed equally to this work.
Editor: Rohit Pappu.

0006-3495/15/09/1190/12
http://dx.doi.org/10.1016/j.bpj.2015.08.011

in disease-associated mutations (12). For example, in the PyrR family of pyrimidine operon attenuators, 11 key allosteric mutations were shown to control the oligomeric state by introducing conformational changes equivalent to the conformational shift between the proteins' free versus nucleotide-bound conformations. On the other hand, hinge axes that were deformed by drug-resistant mutations were subsequently restored by substrate coevolution in HIV-1 protease, implying that the hinge motion of collective fluctuations is important for protein functionality (13).

Computer simulations of protein dynamics should reveal how allosteric communication evolves from the physics of interatomic interactions, ranging from local interactions to collective motions related to functionality. The dynamics is orchestrated through a rearrangement of residue interactions, of which topology is an important determinant (14–17). Here, we first analyzed the dynamics of allosteric mutations in the Structural Database of Kinetics and Energetics of Mutant Protein Interactions (SKEMPI) (18) to reveal a plausible correlation between allosteric mutations of high-binding-affinity changes and global-mode hinges. We then performed studies in human growth hormone (hGH) and pyrin domain (PYD) to determine how an allosteric effect could be viewed by changes in local interactions and global dynamics, and how a perturbation at a hinge site could have a long-range effect on binding behavior. In both cases, we found that mutations were associated with a global mode, i.e., a global-mode perturbation, through local changes in chemistry and/or interactions.

MATERIALS AND METHODS

SKEMPI data set analysis

SKEMPI (18) lists experimentally determined affinities (K_D) in molar (M) for both wild-type and mutant structures. The free-energy changes upon binding and mutation (ΔG and $\Delta\Delta G$, in kcal/mol) are calculated using Eqs. 1 and 2, respectively:

$$\Delta G = RTln(K_D) \quad (1)$$

$$\Delta\Delta G = \Delta G_{mutant} - \Delta G_{wild} \quad (2)$$

where R is the ideal gas constant (8.314 J K^{-1} mol^{-1}), T is the experimental temperature (in K), and K_D is the experimentally measured dissociation constant. Negative and positive $\Delta\Delta G$ values imply stabilizing and destabilizing effects, respectively. The residue locations of mutations in the database are classified as rim, core, or support for residues at the interface, and as interior or surface for noninterface residues (19).

The original data set in SKEMPI (18) includes 3047 entries for binding free-energy changes upon mutation from experimental mutagenesis studies. For our initial data set in this study, we used a more recent version of SKEMPI in which certain entries were eliminated, as described by Dehouck et al. (20). This set excludes 87 reverse mutations, 717 multiple mutations (a single entry with multiple mutants that may contribute simultaneously to a change in affinity), and 236 experimentally redundant entries (more than one experiment for a mutant residue, for which the average $\Delta\Delta G$ value is used). The resulting set contains 2007 mutations in 108 chains of 81 Protein Data Bank (PDB) (21) structures. The redundancies caused by the mutation of a residue into several different residues were further eliminated to obtain a final set composed of 1064 nonredundant mutations in 108 chains of 81 PDB structures (see Supporting Materials and Methods in the Supporting Material). Of these 1064 mutations, 227, 394, and 160 are located at the rim, core, and support of the interface, respectively, and 187 and 96 are located at the surface and interior of the noninterface (allosteric) region, respectively.

We considered different scenarios to explore the association of 283 nonredundant allosteric mutations with hinge regions and the binding free-energy change. For this purpose, we predicted the hinge residues of the structures in the final nonredundant data set for the first two global modes of motion using the Gaussian network model (GNM) (see below), and analyzed the correlation with the energy change upon mutation for different energy thresholds. We also took into account the nearby residues of hinge sites such that their α-carbon distances to hinge residues are within 6 Å in space and they are the first two and three neighbors of hinge residues in sequence (a virtual bond angle in reduced representation is defined by four successive α-carbon atom positions). Then, mutations were mapped to hinge/nearby residues and 20 different energy thresholds (between 0.1 and 2.0 kcal/mol, in increments of 0.1) were considered for the absolute value of the change in the binding free energy upon mutation. For each energy threshold, we evaluated the significance of the correspondence of mutations to hinge/nearby residues below and above the threshold by using the p-value that resulted from Fisher's exact test on a 2×2 contingency table using Python's fisher_exact function in the scipy.stats module (22) (see Supporting Materials and Methods).

Lastly, to test for a bias in the algorithm we used to map mutations to hinge/nearby residues, we generated 1000 sets of random sites in the same number of hinges predicted by the GNM for each PDB chain in the data set. We then repeated the analysis for these 1000 pseudo-hinge/nearby residue sets for all of the threshold values (generating 1000×20 data points).

GNM

The GNM (23,24) is an elastic network model in which a protein is represented as a network of amino acids, where α-carbon atoms are nodes, and edges are the springs (with a uniform force constant γ) combining residues within a cutoff distance (r_{cut}). Residues in the network are assumed to undergo Gaussian-distributed fluctuations around their mean positions. GNM normal modes (mean-square residue fluctuations and correlations between residue fluctuations) can be calculated by diagonalizing the Kirchhoff connectivity matrix. The eigenvalues of the connectivity matrix are proportional to the frequency of motion in the corresponding mode. There are N-1 normal modes, where N is the residue number. Low-frequency (slow) modes represent global functional motions, whereas high-frequency (fast) modes refer to localized fluctuations. A hinge site is defined as the point at which there is a change in the sign of correlation values in a given slow mode (25) and the hinge points mostly overlap the minima of the corresponding slow-mode shape. A hinge site is then composed of successive hinge residues (two or more residues if the hinge site is a short, flexible fragment). In the GNM calculations, r_{cut} was taken as 10 Å and the calculations were done via Python 2.7 (22).

Anisotropic network model

The anisotropic network model (ANM) (26) is an extension of the GNM in which the fluctuations are anisotropic (depending on direction) and the X, Y, and Z components of the position vector, R_i, are incorporated independently. In the ANM, the Kirchhoff connectivity matrix of the GNM is replaced by the Hessian matrix H of the second derivative of the intramolecular potential function (V). H is a symmetric matrix composed of $N \times N$ super elements H_{ij} (each 3×3 in size), given by the second derivatives of V with respect to R_i and R_j of α-carbon atoms of residues i and j, respectively. The

Hessian is decomposed to yield $3N$-6 nonzero eigenvalues and corresponding eigenvectors. In the ANM calculations, r_{cut} is taken as 18 Å.

Molecular-dynamics simulations

For hGH, the starting structure was the wild-type hGH (PDB ID: 1HWG) (27). An in silico hGH mutation, I58A, was created using VMD 1.9.1 (28). Although the crystal structure of hGH in the data set is 1A22 (Table 1), 1HWG was used with 95.6% sequence identity and a 0.62 Å root mean-square deviation (RMSD) to 1A22 (with structural alignment by the jFATCAT rigid algorithm (29)). This structure has only one missing loop, compared with two missing loops in 1A22. We modeled the loop via Mod-Loop (30) using 1HGU, which contains the missing loop as the template. We then minimized the modeled structure using NAMD 2.7 (31) and verified the model quality via Molprobity (32).

PYD complexes of the type I interaction mode were taken from the cryo-electron microscopy (cryo-EM) structure (PDB ID: 3J63) for the PYD dimer and PYD trimer, and for their D48A mutants. The isolated PYD monomer was taken from the full-length NMR structure of ASC (PDB ID: 2KN6) (33). The details of the molecular-dynamics (MD) simulations are given in Table S4.

MD simulations were carried out with the all-atom CHARMM27 force field (34) of NAMD 2.7 (31) using a 2 fs integration time step, with periodic boundary conditions. The temperature was maintained at 310 K with a Langevin damping coefficient of 1 ps^{-1} (35). The pressure was kept at 101.3 kPa by means of Nosé-Hoover Langevin piston pressure control. The SHAKE algorithm was used to restrain the length of bonds involving hydrogen atoms for a time step of 2 fs (36). The initial crystal structures were immersed in a TIP3P-type water box (37) with at least 10 Å of padding between the solute and the edge of the box. The system was neutralized with Cl^- and Na^+ ions. A nonbonded cutoff of 12 Å was used for all Lennard-Jones interactions with a switching function starting at 10 Å, and the long-range electrostatics was treated according to the particle-mesh Ewald method (38). The nonbonded pair list distance was 14 Å. All systems were energetically minimized by the conjugated gradient method for steric crush and crystal contact removal. The trajectories generated by MD simulations were saved every 10 ps for structural and dynamic properties. The analyses were performed using VMD 1.9.1 (28) and all additional calculations were done using MATLAB version R1025a (The MathWorks, Natick, MA). Details regarding the MD trajectory analyses, including calculations of the RMSD profiles, dihedral angle distributions, residue fluctuations, principal component analysis, and hydrogen (H)-bonds, are provided in Supporting Materials and Methods.

TABLE 1 Mapping allosteric mutations with $|\Delta\Delta G| \geq 1$ kcal/mol to hinge/nearby residues

PDB ID_Chain ID_Residue Name, Res. No, Mutant Res. Name	Location	$\Delta\Delta G$ (kcal/mol)	Mode 1 Global Hinges	Mode 2 Global Hinges
1FFW_A_F111V	INT	6.705	110, **111**	
1FC2_C_I135W	INT	3.135	133, 134	
1EMV_A_V68A	INT	1.855		70, 71
1A22_A_I58A	INT	1.637	57, **58**	
3NPS_A_F94A	INT	1.594	**94**, 95	
1KTZ_B_E75A	INT	1.525	**75**, 76	
2C0L_A_Q586R	INT	1.485		584, 585
1KTZ_B_F110A	INT	1.377	112, 113	
1KTZ_B_M112A	INT	1.317	**112**, 113	
1GC1_C_Y82A	INT	1.289		81, **82**
1GC1_C_L51A	INT	1.233	–	–
1JTG_A_K234A	INT	1.221	233, **234**	
1FY8_E_Q156K	INT	1.17	157, 158	
1A22_B_V325A	INT	1.141		322, 323
1KTZ_B_V62A	INT	1.093	63, 64	
1A22_A_F10A	INT	1.039		8, 9
2G2U_B_S130K	INT	−1.468		129, **130**
1E96_A_D38N	SUR	2.2		39, 40
1JRH_H_D55A	SUR	1.665	–	–
1XD3_B_E51A	SUR	1.533		49, 50
3NPS_A_D217A	SUR	1.466		**217**, 219
1FFW_A_V108M	SUR	1.13	110, 111	
1A22_B_D332A	SUR	1.085	330, 331	
1LFD_A_D94K	SUR	−1.146	95, 96	

Non-interface regions are designated as INT (interior) and SUR (surface). If a mutant residue corresponds to a hinge residue in the first two slowest modes, the hinge residue is shown in bold.

RESULTS AND DISCUSSION

Dynamic infrastructure couples allosteric mutations to binding behavior

In general, the strength of receptor-ligand or protein-protein interactions can be characterized by the binding affinity. High binding affinity and specificity imply strong intermolecular forces and a lower free energy of binding, which is not only a local but also a global behavior. The binding phenomenon describes a state in which a complex structure with all its parts maintains dynamical movements for function, highlighting the importance of noninterface regions.

Differences between wild-type and mutant proteins in terms of the free energy of binding can be determined by experimental mutagenesis studies (39) and also by various computational methods, albeit with a relatively lower level of confidence (20,40,41). Many models have been developed to predict the effect of interface residue mutations on binding affinity, but they remain incomplete with respect to allosteric contributions (42). The position of mutations in SKEMPI (18), along with the corresponding binding-affinity changes upon mutation ($\Delta\Delta G$), shows that interface residues are significantly responsible for large affinity changes, and core residues are the most effective ones. Nevertheless, only a small group of allosteric residues contribute significantly to the binding free energy, so we chose to utilize this group in our study.

We explored the structural dynamics of 108 chains on 81 PDB structures by using the GNM to identify hinge and nearby residues that define the dynamic domains of the slowest and second-slowest modes of motion (23,24) (see Materials and Methods and the hGH and PYD case studies for details). On average, only 12.2% of residues were found to be at hinge sites (Table S1). Although hinge residues may be sparse in sequence, their order in the structure can be used to define dynamic domains and coordinate global motion (see Figs. 2 and 4). We mapped 283 allosteric mutations out of 1064 nonredundant mutations in the final data set (see Supporting Materials and Methods for details of the data set) to predicted hinges/nearby residues to reveal a plausible correspondence between the amount of change

in the binding free energy upon mutation for different energy thresholds (Fig. 1; Table S2).

We found that the nonredundant allosteric mutations in SKEMPI (18) significantly corresponded to hinge/nearby residues above the energy thresholds, and to residues other than hinge/nearby residues below the energy thresholds in the range of 0.6–1.5 kcal/mol (Fig. 1, *A* and *B*, *red bars with star*; Table S2, *green cells*). For larger threshold values ($\geq$1.6 kcal/mol), a smaller number of mutations in the sample set led to an increased probability of random correspondence to a hinge/nearby residue. For example, there were three allosteric mutations with binding free-energy change values >2 kcal/mol, and although all of them corresponded to hinge/nearby residues, this correspondence was found to be insignificant (Fig. 1, *A* and *B*; Tables 1 and S2). On the other hand, for smaller thresholds ($\leq$0.5 kcal/mol), the mutations did not significantly prefer hinge/nearby residues either. This is due to the rapid increase in the number of mutations, with the energies overcoming the threshold (while the number of hinge/nearby residues did not change), leading to lower probabilities for hinge/nearby-residue correspondence (Fig. 1, *A* and *B*; Table S2). The latter observation implies that the residues whose mutations cause a low binding free-energy change are not likely to correspond to important structural positions such as hinge/nearby residues.

We then elaborate on an example binding free-energy change threshold of 1 kcal/mol, for which the hinge/nearby-residue preference of mutations is most significantly imbalanced below and above the threshold (*p*-value of 1.72e-05 in Fisher's exact test; Fig. 1 *B*; Table S2). The results show that 139 of 259 nonredundant allosteric mutations with binding free-energy changes below the threshold ($|\Delta\Delta G| < 1$ kcal/mol) significantly correspond to residues other than hinge/nearby (first two neighbors in sequence) residues, whereas 22 of 24 mutations above the threshold ($|\Delta\Delta G| \geq 1$ kcal/mol) map significantly to hinge/nearby residues (Fig. 1 *B*; Tables 1 and S2). Note that only two cases do not match hinge/nearby residues, and one of them (PDB ID: 1JRH, D55A mutant) is a hinge residue in the third-slowest GNM mode.

If we consider only hinge residues (exact positions), there is still a significant correspondence of mutations to hinge residues above the threshold and residues other than hinge residues below the energy thresholds in the range of 1.2–1.4 kcal/mol (Fig. 1 *C*, *red bars with star*; Table S2, *green cells*). However, we observe false positives for the energy thresholds between 0.5 and 1.1 kcal/mol, where mutant residues significantly correspond to residues other than hinge residues both below and above the threshold (Fig. 1 *C*, *red bars without star*; Table S2, *orange cells*). For the smaller and larger energy thresholds, the results are insignificant for reasons similar to those explained above. On the other hand, when the first three neighbors of hinge residues in sequence are considered, the rapid increase in the number of nearby residues leads to false-positive mappings. As such, for the energy thresholds in the range of 0.9–1.5 kcal/mol, although the preference is still significantly imbalanced, the mutations with the energies both below and above the thresholds correspond to hinge/nearby residues (Fig. 1 *D*, *red bars without star*; Table S2, *orange cells*).

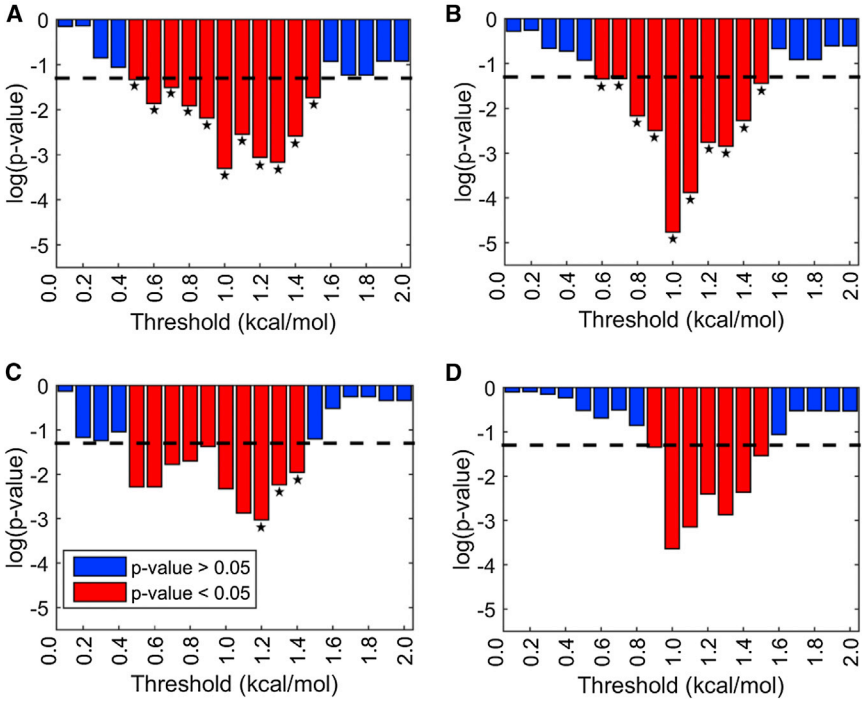

FIGURE 1 Significance of the correspondence of mutations to hinge/nearby residues when the absolute value of the change in the binding free energy upon mutation ($\Delta\Delta G$) is below or equal to/above different thresholds. (*A–D*) Four different cases are studied, with mutations mapped to (*A*) hinge residues with neighbors whose α-carbon distances are within 6 Å in space, (*B*) hinge residues with their first two neighbors in sequence, (*C*) exact positions of hinge residues without nearby residues, and (*D*) hinge residues with their first three neighbors in sequence. Logarithm of *p*-values (calculated in Fisher's exact test) is used for visual purposes (see Table S2 for details of the data analysis). The dotted line shows the *p*-value cutoff for accepting (*blue*) or rejecting (*red*) the initial null hypothesis (95% confidence interval). The star sign indicates true-positive results, where mutant residues significantly correspond to hinge/nearby residues above the threshold, and to residues other than hinge/nearby residues below the threshold. The red bars without a star are false positives, where mutant residues significantly correspond to residues other than hinge residues both below and above the threshold. Note that Fig. S1 is slightly different from this figure and depicts analysis results only for mutations to alanine. To see this figure in color, go online.

Furthermore, to eliminate any impact of the mutant residue type on the binding free-energy change with respect to the correspondence to hinge/nearby residues, we considered only alanine mutations in SKEMPI as a subset and performed the same statistical analyses. Including only the mutations to alanine reduces the *p*-values in Fisher's exact test for the energy thresholds in the range of 0.1–0.8 kcal/mol and thus increases the significance of mapping mutations to hinge/nearby residues (Table S2 versus Table S3). However, the *p*-values are observed to increase for the energy thresholds of 0.9–1.8 kcal/mol. Overall, a significant hinge/nearby-residue correspondence for the mutations with binding free-energy changes above the threshold and significant preference for residues other than hinge/nearby residues below the threshold are observed for the energy thresholds in the range of 0.5–1.3 kcal/mol (Fig. S1, *A* and *B*, *red bars with star*; Table S3, *green cells*). Note that the energy threshold range changes slightly with respect to the previous range observed when non-alanine mutations are also considered (0.6–1.5 kcal/mol). When only hinge residues and the first three neighbors of hinge residues in sequence are considered, the results are also similar (Fig. 1, *C* and *D*, versus Fig. S1, *C* and *D*). These observations indicate that a change of residue type in a mutation does not significantly affect the correlation between the binding free-energy change and whether that residue is on a hinge/nearby-residue site.

Lastly, as a control, we compared the analysis results for the randomly generated hinge sites (described in Materials and Methods) with the hinge sites predicted by the GNM in SKEMPI. The *p*-values are found to be equally distributed and significantly higher in randomly generated data sets, yielding an insignificant correspondence of mutations to hinge/nearby residues in most cases (Fig. S2). The mutations significantly correspond to hinge residues, hinge/6 Å nearby residues, hinge/first two nearby residues, and hinge/first three nearby residues for only 1000, 750, 1500, and 750 out of 20,000 cases (20 thresholds × 1000 randomly generated hinge sets), respectively (Fig. S2). Thus, the results presented here are highly significant with respect to the results based on randomly generated hinge residues.

Hinges on hGH allosterically control receptor-binding sites

I58A is an allosteric mutation on the hinge site of hGH with a large binding free-energy change (Table 1; PDB ID: 1A22). Here, we further examine the mechanism underlying the allosteric dynamics of this mutation. hGH participates mainly in the regulation of normal human growth and development, and other physiological and metabolic processes (43). It binds to a dimerized inactive GH receptor (hGHR) at the target cell's surface to form an active complex, which induces many downstream signaling events (44,45). The protein has a four-helix bundle motif with an up-up-down-down topology, and three additional small helices (Fig. S3 *A*) (27,46). hGH may interact with one (1:1) or two identical (1:2) hGHRs via its two asymmetric binding sites (site 1 (s1) and site 2 (s2); Fig. 2 *A* and *B*) (27,45,47). Yet, hGHR has only one binding region to interact with these two distinct binding sites on hGH (47).

Global modes and hinges

The first two slowest modes of hGH by the GNM (PDB ID: 1HWG) describe the most cooperative motion of hGH (Fig. S3, *B* and *C*), where hinge residues define the dynamic domains (Fig. 2, *C* and *D*). The slowest mode reveals a set of residues forming a hinge plane that bisects the structure into two dynamic domains (Fig. 2 *C*, *blue* and *red*). The second-slowest-mode hinges also divide the structure mainly into two dynamic domains, slightly different than the dynamic domains of the slowest mode hinges (Fig. 2 *D*, *blue* and *red*). When the two slowest modes amalgamate, the prominence of the two hinge planes is relieved. The hinges of the two slowest modes distribute flexible segments across the structure for a plausible allosteric communication, as discussed below.

I58 is one of the hinge residues whose mutation to alanine allosterically reduces the binding affinity of a 1:1 complex with hGHR at s1 by 1.637 kcal/mol (48). This raises the interesting question of how a perturbation introduced by the I58A mutation is disseminated throughout the structure to the binding interface that evidently makes a significant contribution to the binding free energy. Apart from I58, there are other hinge residues that could be associated with the binding behavior: K172 is at the interface, and F54 and V185, as allosteric positions, overlap the mutations that lead to relatively high $\Delta\Delta G$ values. On the other hand, the positions of the remaining hinges of the two slowest modes with low $\Delta\Delta G$ values still may not be false positives, as their mutation to residues other than the ones listed in the data set may result in higher binding free-energy changes, they may overlap some other functional residues, and/or they may be associated with other possible binding sites. To illustrate the structural and dynamic changes of the I58A mutation, we present the results of MD simulations of both the wild-type and in silico I58A hGH below (see Table S4 for simulation details).

Network of correlated fluctuations

The MD simulations reveal that there is no significant structural variation between the wild-type and mutant hGH (Fig. S4 *A*); however, the I58A mutation mainly affects the patterns of dynamic correlations (Figs. S4, *B–E*, and S5). The dynamic correlations of the F54-I58 region, which is a small helix lying between the hinge residues of the slowest and second-slowest modes (Fig. 2, *A* and *B*, respectively), show that there is a highly correlated path (A17-D26, R77-P89, Q137-F146, and N159-F176) to the hGHR interface in the wild-type hGH, which is weakened with the

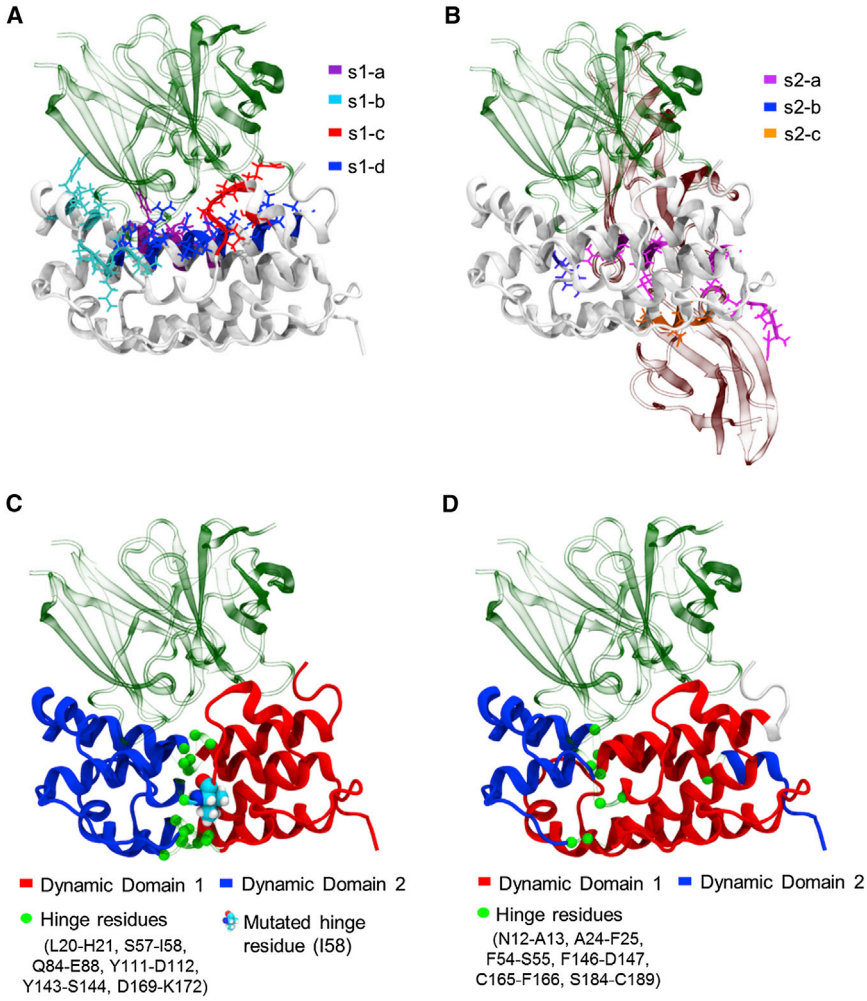

FIGURE 2 Functional sites and hinges/dynamic domains in hGH. (*A*) High-affinity-binding site 1 (s1) on hGH (*white*) in complex with its receptor hGHR (*transparent green*; PDB ID: 1HWG): the middle of helix 1 (s1-a: H18, H21, Q22, and F25), helix 2, and a part of the loop of helix 2-helix 3 (s1-b: K41, Y42, L45, Q46, and Q49-L52), the N-terminus of helix 4 (s1-c: P61-R64 and T67), and the outer surface of the C-terminus of helix 7 (s1-d: Y164, R167, K168, D171, K172, E174, T175, R178, I179, and C182). (*B*) Binding site 2 (s2) in hGH (*white*) with two hGHRs (*transparent green* and *transparent brown*): the N-terminus of helix 1 (s2-a: F1, P2, I4, R8, L9, L15, R16, and R19), the loop of helix 5-helix 6 (s2-b: Y103), and the C-terminal outer surface of helix 6 (s2-c: D116, R119, G120, and T123). (*C* and *D*) Slowest (*C*) and second-slowest (*D*) mode hinges and dynamic domains of hGH (Fig. S3, B and C). To see this figure in color, go online.

I58A mutation. These correlated regions include residues from the s1-a and s1-d binding patches on the high-affinity-binding site, s1 (Fig. 2 *A*). Additionally, s1-c has positively correlated fluctuations with s1-d and negatively correlated fluctuations with s1-b in the wild-type, which are also weakened by the I58A mutation (Fig. 3, *C* and *D*, respectively). These regions encompass eight hot-spot residues (K41 and L45 on s1-b; P61 and R64 on s1-c; and K172, T175, F176, and R178 on s1-d) of 31 binding residues that hold ~85% of the binding energy according to alanine-scanning mutagenesis experiments (29,32). P61A, R64A, K172A, T175A, F176A, and R178A cause a 5- to 30-fold increase in the off-rate of the hGH-hGHR complex. The high negatively correlated fluctuations between s1-b and s1-c could be viewed as a flapping motion to embrace the receptor and/or to open/close the gate to the receptor to bind s1-d in the wild-type hGH.

Backbone movements and H-bonding

The I58A mutation allosterically leads to a change in the distribution of the backbone dihedral angles of F44, N47, Q49-T60, S62, Y103-A105, L128-R134, and A148-A155 (Fig. S6), which include residues from the s1-b, s1-c, and s2-b binding patches (Fig. 2, *A* and *B*). The changes in the backbone movements can be substantiated by the alteration of the H-bond network (Figs. 3 *E* and S7). The I58A mutation mainly disrupts the H-bond network along the hinge residues of the slowest modes or nearby loops. H-bonds that bridge s1-a to s1-d (H21-E174-H18), S85-S144, and W86-D169-K172 are broken, whereas new H-bonds (R16-D116 and S55-D169) are formed (Fig. 3 *E*). Along with this, the disappearance/appearance of some distant H-bonds (Y101-E30-V100 and S62-E66, and N72-R183 and F44-T50, respectively) is also observed. Together with the rearrangement of some backbone dihedral angles, this modifies the ensemble of conformations and leads to the observed changes in the pattern of correlated fluctuations at the binding patches of s1 on hGHR (Figs. 3, *A–D*, and S4).

Furthermore, hGHR was shown to be activated by sequential dimerization, such that hGH binds first to a receptor from s1 and then to a second receptor from s2 (49),

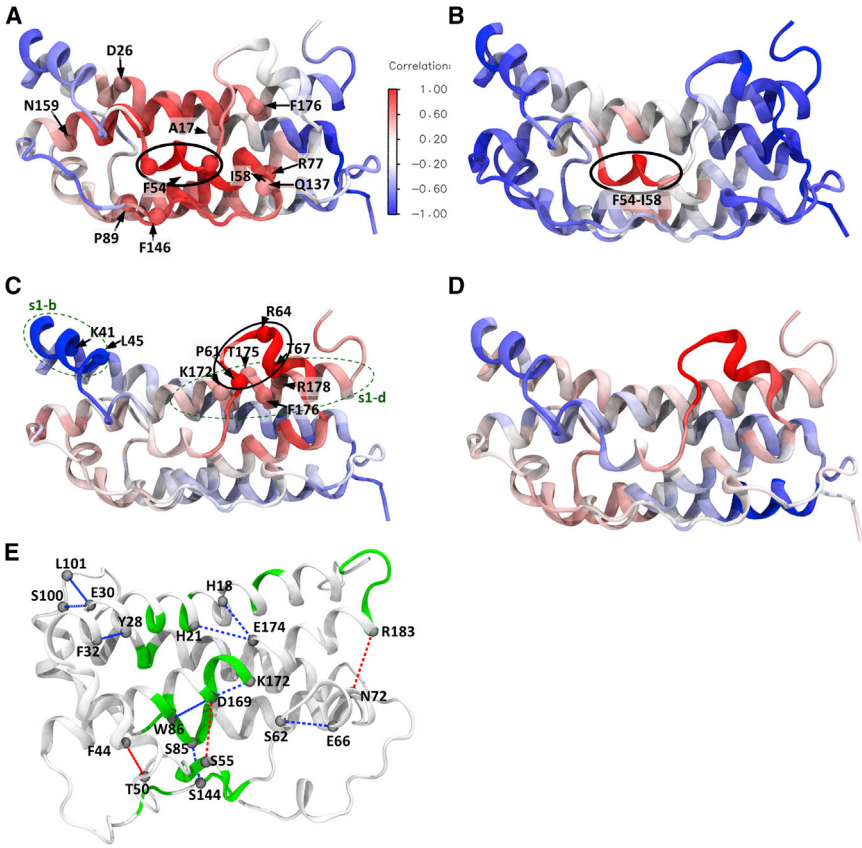

FIGURE 3 Dynamic correlations and H-bonds in hGH. (*A–D*) Correlation of F54-I58 (*A* and *C*, *solid circle*) and the binding site s1-c (*B* and *D*, *solid circle*) with the rest of the structure in wild-type and I58A hGH, respectively; hot-spot residues (29,32) in s1-b, s1-c, and s1-d are labeled (Figs. 2, *A* and *B*). The underlying correlation maps are provided in Fig. S4, *B* and *C*. The H-bonds observed between residue pairs in the wild-type hGH, but not in the I58A hGH, and vice versa, are connected via blue and red dotted lines, respectively, and hinge residues are in green (*E*). To see this figure in color, go online.

implying an allosteric communication between the two binding sites. The I58A mutation also changes the dihedral angle distribution of s2 on hGHR (residues Y103-A105) along with the breaking of an H-bond network (Y101-E30-V100) in s2-b and the formation of H-bonds between s2-a and s2-c (R16-D116). This decreases the dynamic coupling between two regions (E80-T89 and K109-R119), which includes the slowest-mode hinges Q84-L88 and Y111-D112 (Fig. S4, *B* and *C*). As s1-a/s1-d also display reduced correlations with E80-T89 upon the I58A mutation, this may allosterically affect the interaction between the two hGHR-binding sites.

Hinges control alternative interaction modes in PYD-PYD filaments

The activation of NLRP3, NLRC4, and AIM2 inflammasomes is known to be complemented by the rapid formation of a micrometer-sized and insoluble perinuclear structure called an ASC speck (apoptosis-associated Speck-like protein containing CARD), which acts as an adaptor (50–52). ASC protein consists of N-terminal PYD and C-terminal CARD (Caspase activation and recruitment domain) connected by a flexible linker (33). ASC specks are not simply structures that result from nonspecific aggregation of individual ASC proteins; rather, they interact via hydrophobic patches of specific interactions of PYDs and CARDs (52,53). Both PYD and CARD belong to the death-fold superfamily, and overexpression of PYD and CARD separately forms filament structures. Three different interaction modes (types I, II, and III) were suggested for PYD-filament formation (Fig. 4 *A*) (52–55). All three of these interaction modes have basically two surfaces to mediate PYD-PYD interactions. The type I interaction mode is mediated by helices H1/H4 and helices H2/H3, the type II interaction mode occurs between the loops of H4/H5 and H5/H6, and the type III interaction mode occurs between the H1/H2 loop and H3 (53–55).

The type I interaction mode was believed to act in oligomerization via a charge-charge interaction across the interface of two neighboring PYD monomers through helices H1/H4 of one monomer and helices H2/H3 of the other (55). However, MD simulations of the wild-type and the D48A PYD monomer (PDB: 2KN6) showed that the two binding surfaces of the type I interaction mode are allosterically coupled in their fluctuations, suggesting a plausible control between the two surfaces of the type I interaction mode and the existence of alternative interaction modes (Fig. S8, *A* and *B*) (52). With the D48A mutation at a position predicted as a global hinge of the PYD monomer, the dynamic correlation between the type I interaction mode

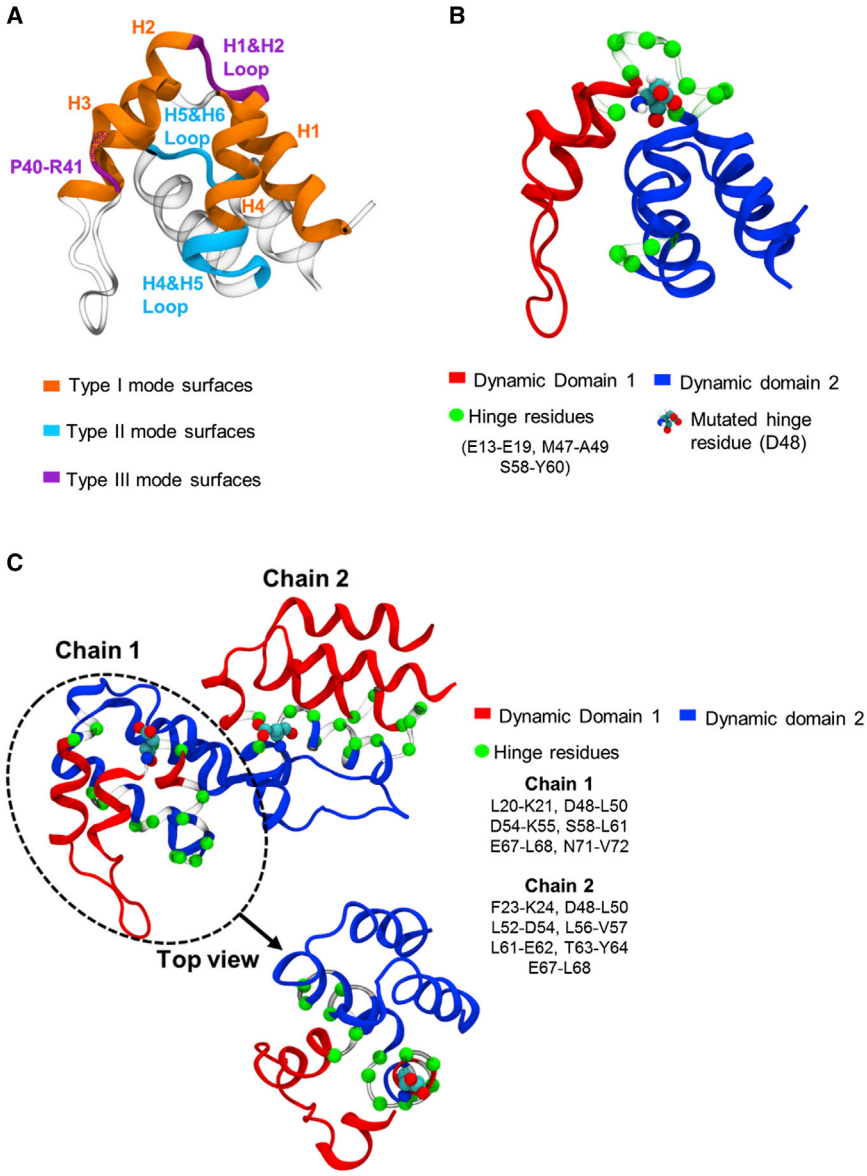

FIGURE 4 Binding modes and hinge residues of PYD. (*A*) Three types of interaction mode surfaces of the PYD monomer (PDB ID: 2KN6). (*B*) Slowest-mode hinges of the PYD monomer with dynamic domains. (*C*) Second-slowest-mode hinges with the dynamic domains of the PYD dimer (Fig. S9). D48 is shown as spheres colored by atom types. To see this figure in color, go online.

surfaces decreased, whereas it increased for the other two interaction mode surfaces (Fig. S8, *A* and *B*) (52). The latter finding is further supported by the inhibition of the PYD filament formation with the D48A mutation and colocalization of the D48A PYDs on the wild-type PYDs in an in vivo mutational analysis.

Global modes and hinges

D48 is one of the hinge residues predicted by the slowest mode of the PYD monomer (52) and the second-slowest mode of the PYD dimer interacting via the type I interaction mode (Figs. 4, *B* and *C*, and S9 *B*). Although this residue was initially suggested to participate in PYD oligomerization through a charge-charge interaction across the interface interactions (55), a direct interaction of the two PYDs is not observed in the recent cryo-EM structure (53). The D48A mutation disrupts the type I interaction mode and exposes the other types of interaction modes (Fig. S8, *A* and *B*). The D48 position is important because of its capacity to disseminate a global effect through a perturbation in the global dynamic mode in the PYD monomer and dimer (Figs. 4, *B* and *C*, and S9 *B*). Further, S58-E62 residues at the H4/H5 loop of the type II interaction mode are also found to be associated with the global hinges in the PYD monomer (slowest mode) and dimer (second-slowest mode; Fig. 4, *B* and *C*). We also observe that the slow-mode hinges of the PYD dimer overlap those of the PYD monomer, to which a previous study ascribed some functional roles (52).

Here, to extend the analysis of the previous PYD monomer MD simulations (52), we performed MD simulations of the PYD dimer of the type I interaction mode from the

cryo-EM structure (PDB ID: 3J63) together with its D48A mutant (Table S4).

Oligomerization over type I predisposes other types of interaction modes in PYD

The correlations between residue fluctuations (i.e., dynamic coupling) over six parallel MD simulations of the PYD dimer (Figs. S10, *B–F*, and S11) with respect to the isolated PYD monomer reveal an interplay between different interaction modes. Details of the MD simulations are given in Table S4.

The two surfaces of the type I interaction mode are allosterically coupled within the isolated PYD monomer, which means that these two surfaces communicate with each other (52). In the PYD dimer, the two surfaces of the type I interaction mode are coupled in two ways: locally at the interface and allosterically between the two unoccupied surfaces of the monomers (Figs. 5 *A* and S10 *B*). With respect to chain 1, H1 of chain 1 correlates with H2, H3, and the C-terminus H5 of chain 2 at the interface, and also with H4, the H4/H5 loop, the N-terminus of H5, and the C-terminus of H6 of chain 1. On the other hand, H1 of chain 2, which is allosteric to the interface, displays long-distance dynamic correlations with the unoccupied type I interaction mode surface of chain 1, particularly with H2 and the C-terminus of H5. The prion-like nature of the PYD-PYD oligomerization may be supported with these distant dynamic correlations (56). Once dimerization is achieved through one of the type I interaction mode surfaces of a PYD monomer, further oligomerization can be achieved through the unoccupied surfaces of the type I interaction modes of both chains 1 and 2. Coupling between the type I interaction mode surfaces of the PYD dimer, both at the interface and at the unoccupied surfaces, is weakened with the D48A PYD dimer (Figs. 5 *B* and S10 *C*). Apparently, this mutation unsettles the PYD polymerization of the type I interaction mode by leading to an altered ensemble of conformations. The D48A PYD dimer obtained via the type I mode of interaction may not be a physiologically observable state (48), but is presented here to show that even when dimerization is achieved via the type I mode of interaction, D48A mutations change the network of correlations within the protein.

Type II interaction mode surfaces (the H4/H5 and H5/H6 loops) are weakly coupled in the PYD monomer's dynamics, which becomes stronger with the D48A mutation (Fig. S8 *B*) (52). On the other hand, a strong dynamic coupling between the type II interaction mode surfaces of the two chains of the PYD dimer is observed (Fig. 5, *C* and *D*). The H5/H6 loop of chain 1 correlates with the H4/H5 loop of chain 2, along with H2 of chain 1 and H4 of chain 2 (Fig. 5 *C*). Moreover, the H4/H5 loop of chain 1 also correlates with the H5/H6 loop of chain 2 (Fig. 5 *D*).

No dynamic correlation is observed between the surfaces of the type III interaction mode (P40-A43 on H3 at one surface and the H1/H2 loop on the other) in the PYD monomer, which appears with the D48A mutation (52). In the PYD dimer, the dynamic correlation of the two type III interaction mode surfaces appears only within the H1/H2 loop of chain 1 and P40-A43 of chain 2 (Fig. 5 *E*). However, the reciprocal of this coupling from chain 2 to chain 1 with the respective surfaces is not observed (Fig. 5 *F*). Interestingly, instead the H1/H2 loop of chain 2 is correlated with the H4/H5 loop of chain 1, implying a possible coupling among type II and type III interaction modes.

These correlations indicate that once the type I interaction mode is assumed through a dimerization, the correlation between the two surfaces of the type II and/or type III interaction modes are enhanced for further assembly. With dimerization, the additional contacts that form at the interface between the monomers mainly help the PYD chains to induce the other interaction modes, as in the D48A PYD monomer. The interface should have an impact on (i.e., perturb) the global hinge at D48, which may have an effect on the cooperative motions involving the dynamic couplings between the surfaces of various interaction modes. The latter notion reflects the experimental observation that the D48A mutant PYD is colocalized with the wild-type PYD (52), and implies that this occurs through the type II and type III interaction mode surfaces.

Backbone movements and H-bonding

In the PYD monomer, the D48A mutation breaks the H-bonds between the N-terminus of H1 and the H4/H5 loop (M1-E62-R3), which is one of the binding surfaces of the type II interaction mode (Figs. 5 *G* and S12). Along with this, a change in the distribution of the backbone dihedral angles of residues Y60 and L61 appears that affects the conformational space of the H4/H5 loop (Figs. S12 and S13). Interestingly, the same H-bonds are broken in both chains of the PYD dimer, leaving E62 free to interact with its partner PYD. The disappearance of these H-bonds is thus significant in the emergence of the type II interaction mode via either a D48A mutation in the monomer or dimerization over the type I interaction mode. The H4/H5 loop and D48 of both chains are associated with the hinge residues of the second-slowest mode of the PYD dimer, as well as the slowest mode of the PYD monomer (Fig. 4, *B* and *C*). This implies that a perturbation at D48 may affect the associated global motion, where the H4/H5 loop is also part of the dynamic infrastructure.

CONCLUSIONS

The coupling of local interactions to global motion appears to be essential for functionality. Although various network models have been developed in an attempt to explain the dissemination of a local perturbation in a structure, the mechanisms underlying local to global changes remain elusive. Dynamically fluctuating conformational ensembles and a shift in the ensemble of distributions provide a view of

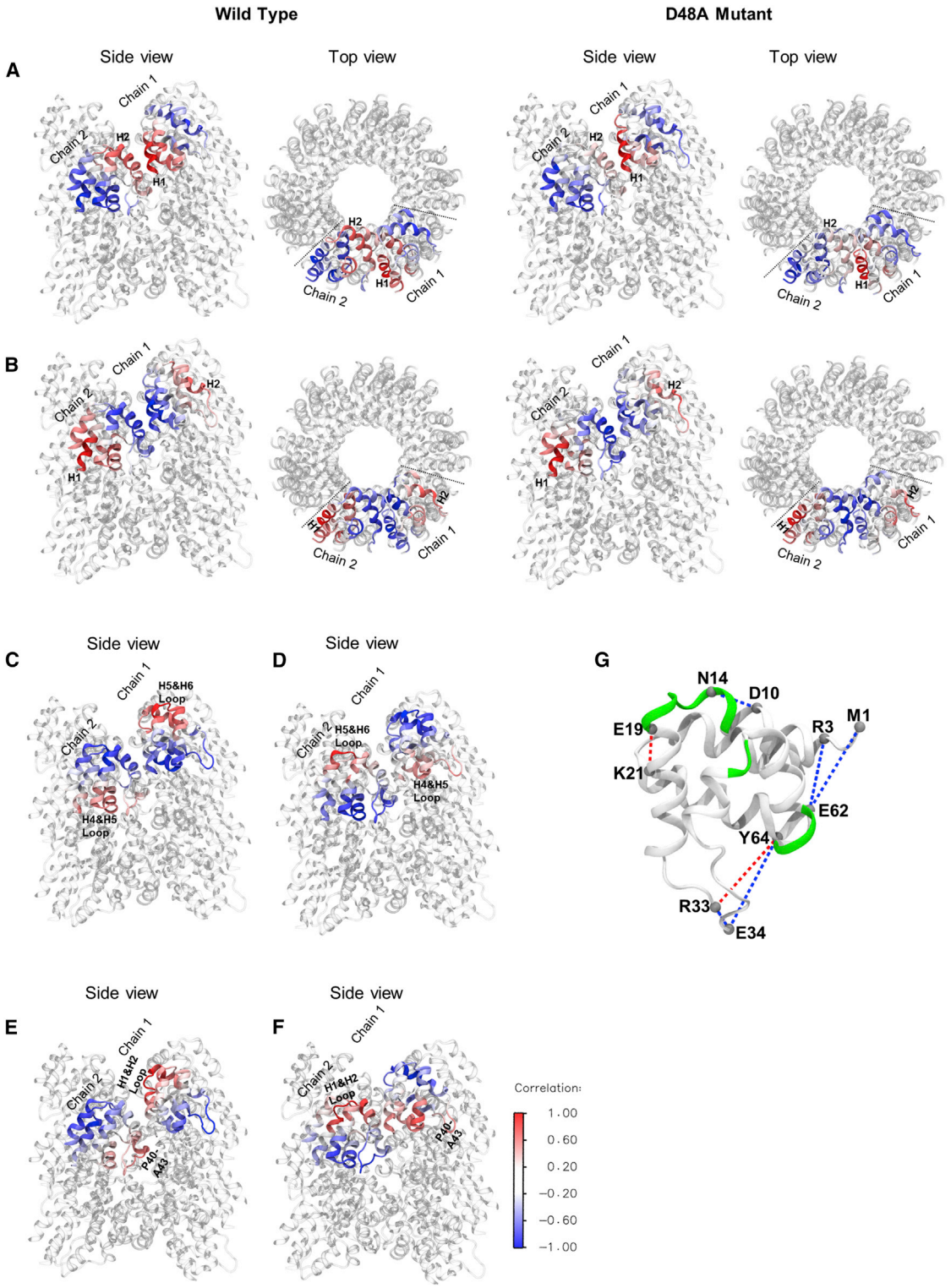

FIGURE 5 Dynamic correlations in the PYD dimer interacting via type I interaction mode surfaces and H-bonds on the PYD monomer. (*A* and *B*) Correlation of H1 of chain 1 (*A*) and H1 of chain 2 (*B*) with the rest of the PYD dimer for the wild-type and D48A. (*C* and *D*) Correlation of the loop of H5/H6 of chain 1 (*C*) and the loop of H5/H6 of chain 2 (*D*) with the rest of the PYD dimer for the wild-type, revealing the cooperativity between type II interaction mode surfaces. (*E* and *F*) Correlation of the loop of H1/H2 of chain 1 (*E*) and the loop of H1/H2 of chain 2 (*F*) with the rest of the PYD dimer, revealing the cooperativity between type III interaction mode surfaces. The PYD dimer is taken from the cryo-EM structure (PDB ID: 3J63). The underlying correlation maps are presented in Fig. S10, *B* and *C*. (*G*) The H-bonds observed between residue pairs in the wild-type, but not in the D48A PYD monomer, and vice versa, are connected by blue and red dotted lines, respectively, and hinge residues are in green. To see this figure in color, go online.

allosteric events with local physical/chemical changes. The populations of conformational states are most effectively modulated by global-mode hinges. Any change at a hinge region leads to the modification of some of the bonding interactions, followed by backbone rearrangements and an alteration in the sampling of the conformational space. This results in a global effect that disposes allosteric pathways and interactions with conformational changes and/or dynamics. This is intimately related to the topology of the structure, which makes a residue with this capacity a hinge site that affects the dynamic energy landscape.

In this context, the significant association between the hinge positions of global modes and allosteric mutations that lead to high-binding-affinity changes is reminiscent of a dynamic infrastructure that is built in accord with the binding behavior, as elucidated by the dynamics of hGH. Further, since a hinge has the dynamic ability to expose intrinsic alternative binding modes, there could be an interplay between accessible binding modes as presented in the PYD dimer with respect to the isolated wild-type and mutant PYD monomer. This interplay also implies an order in the helical assembly of PYDs, which may lead to, higher-order assemblies.

Hinge sites are thus plausible sites for deciphering the hidden functional potential embedded in structural dynamics and modulating protein-protein interactions.

SUPPORTING MATERIAL

Supporting Materials and Methods, thirteen figures, and four tables are available at http://www.biophysj.org/biophysj/supplemental/S0006-3495(15)00822-X.

AUTHOR CONTRIBUTIONS

T.H., F.S., and S.E.A.-O. designed the research. F.S. and S.E.A.-O. performed the research. F.S. and S.E.A.-O. analyzed the data. T.H., F.S., and S.E.A.-O. wrote the manuscript.

ACKNOWLEDGMENTS

This work was supported by the Scientific and Technological Research Council of Turkey (grant number 112T569).

SUPPORTING CITATIONS

References (57–60) appear in the Supporting Material.

REFERENCES

1. Bahar, I., and A. J. Rader. 2005. Coarse-grained normal mode analysis in structural biology. *Curr. Opin. Struct. Biol.* 15:586–592.
2. Weinkam, P., Y. C. Chen, …, A. Sali. 2013. Impact of mutations on the allosteric conformational equilibrium. *J. Mol. Biol.* 425:647–661.
3. Ma, B., C. J. Tsai, …, R. Nussinov. 2011. Dynamic allostery: linkers are not merely flexible. *Structure.* 19:907–917.
4. Laskowski, R. A., F. Gerick, and J. M. Thornton. 2009. The structural basis of allosteric regulation in proteins. *FEBS Lett.* 583:1692–1698.
5. Nussinov, R., C. J. Tsai, and J. Liu. 2014. Principles of allosteric interactions in cell signaling. *J. Am. Chem. Soc.* 136:17692–17701.
6. Korkmaz, E. N., R. Nussinov, and T. Haliloğlu. 2012. Conformational control of the binding of the transactivation domain of the MLL protein and c-Myb to the KIX domain of CREB. *PLOS Comput. Biol.* 8:e1002420.
7. Nussinov, R., and C. J. Tsai. 2015. Allostery without a conformational change? Revisiting the paradigm. *Curr. Opin. Struct. Biol.* 30:17–24.
8. Kuriyan, J. 2004. Allostery and coupled sequence variation in nuclear hormone receptors. *Cell.* 116:354–356.
9. Henzler-Wildman, K., and D. Kern. 2007. Dynamic personalities of proteins. *Nature.* 450:964–972.
10. Hines, C. S., K. Ray, …, D. W. Rodgers. 2014. Allosteric inhibition of the neuropeptidase neurolysin. *J. Biol. Chem.* 289:35605–35619.
11. Gerek, Z. N., and S. B. Ozkan. 2011. Change in allosteric network affects binding affinities of PDZ domains: analysis through perturbation response scanning. *PLOS Comput. Biol.* 7:e1002154.
12. Nevin Gerek, Z., S. Kumar, and S. Banu Ozkan. 2013. Structural dynamics flexibility informs function and evolution at a proteome scale. *Evol. Appl.* 6:423–433.
13. Özer, N., A. Özen, …, T. Haliloğlu. 2015. Drug-resistant HIV-1 protease regains functional dynamics through cleavage site coevolution. *Evol. Appl.* 8:185–198.
14. Lockless, S. W., and R. Ranganathan. 1999. Evolutionarily conserved pathways of energetic connectivity in protein families. *Science.* 286:295–299.
15. Pan, H., J. C. Lee, and V. J. Hilser. 2000. Binding sites in Escherichia coli dihydrofolate reductase communicate by modulating the conformational ensemble. *Proc. Natl. Acad. Sci. USA.* 97:12020–12025.
16. Tsai, C. J., A. del Sol, and R. Nussinov. 2008. Allostery: absence of a change in shape does not imply that allostery is not at play. *J. Mol. Biol.* 378:1–11.
17. Hilser, V. J. 2010. Biochemistry. An ensemble view of allostery. *Science.* 327:653–654.
18. Moal, I. H., and J. Fernández-Recio. 2012. SKEMPI: a structural kinetic and energetic database of mutant protein interactions and its use in empirical models. *Bioinformatics.* 28:2600–2607.
19. Levy, E. D. 2010. A simple definition of structural regions in proteins and its use in analyzing interface evolution. *J. Mol. Biol.* 403:660–670.
20. Dehouck, Y., J. M. Kwasigroch, …, D. Gilis. 2013. BeAtMuSiC: prediction of changes in protein-protein binding affinity on mutations. *Nucleic Acids Res.* 41:W333–W339.
21. Berman, H. M., J. Westbrook, …, P. E. Bourne. 2000. The Protein Data Bank. *Nucleic Acids Res.* 28:235–242.
22. Oliphant, T. E. 2007. Python for scientific computing. *Comput. Sci. Eng.* 9:10–20.
23. Bahar, I., and R. L. Jernigan. 1998. Vibrational dynamics of transfer RNAs: comparison of the free and synthetase-bound forms. *J. Mol. Biol.* 281:871–884.
24. Haliloglu, T., I. Bahar, and B. Erman. 1997. Gaussian dynamics of folded proteins. *Phys. Rev. Lett.* 79:3090.
25. Emekli, U., D. Schneidman-Duhovny, …, T. Haliloglu. 2008. HingeProt: automated prediction of hinges in protein structures. *Proteins.* 70:1219–1227.
26. Atilgan, A. R., S. R. Durell, …, I. Bahar. 2001. Anisotropy of fluctuation dynamics of proteins with an elastic network model. *Biophys. J.* 80:505–515.
27. Sundström, M., T. Lundqvist, …, G. Norstedt. 1996. Crystal structure of an antagonist mutant of human growth hormone, G120R, in complex with its receptor at 2.9 A resolution. *J. Biol. Chem.* 271:32197–32203.
28. Humphrey, W., A. Dalke, and K. Schulten. 1996. VMD: visual molecular dynamics. *J. Mol. Graphics.* 14:33–38, 27–38.

29. Ye, Y., and A. Godzik. 2003. Flexible structure alignment by chaining aligned fragment pairs allowing twists. *Bioinformatics.* 19 (*Suppl 2*):ii246–ii255.

30. Fiser, A., R. K. Do, and A. Sali. 2000. Modeling of loops in protein structures. *Protein Sci.* 9:1753–1773.

31. Phillips, J. C., R. Braun, …, K. Schulten. 2005. Scalable molecular dynamics with NAMD. *J. Comput. Chem.* 26:1781–1802.

32. Chen, V. B., W. B. Arendall, 3rd, …, D. C. Richardson. 2010. MolProbity: all-atom structure validation for macromolecular crystallography. *Acta Crystallogr. D Biol. Crystallogr.* 66:12–21.

33. de Alba, E. 2009. Structure and interdomain dynamics of apoptosis-associated speck-like protein containing a CARD (ASC). *J. Biol. Chem.* 284:32932–32941.

34. Brooks, B. R., R. E. Bruccoleri, …, M. Karplus. 1983. CHARMM: a program for macromolecular energy, minimization, and dynamics calculations. *J. Comput. Chem.* 4:187–217.

35. Levy, R. M., M. Karplus, and J. A. McCammon. 1979. Diffusive Langevin dynamics of model alkanes. *Chem. Phys. Lett.* 65:4–11.

36. Ryckaert, J. P., G. Ciccotti, and H. J. C. Berendsen. 1977. Numerical integration of the Cartesian equations of motion of a system with constraints: molecular dynamics of *n*-alkanes. *J. Comput. Phys.* 23:327–341.

37. Jorgensen, W. L. 1983. Comparison of simple potential functions for simulating liquid water. *J. Am. Chem. Soc.* 103:335–340.

38. Darden, T., D. York, and L. Pedersen. 1993. Particle mesh Ewald: an N•log (N) method for Ewald sums in large systems. *J. Chem. Phys.* 98:10089–10092.

39. Fersht, A. R. 1987. Dissection of the structure and activity of the tyrosyl-tRNA synthetase by site-directed mutagenesis. *Biochemistry.* 26:8031–8037.

40. Pires, D. E., D. B. Ascher, and T. L. Blundell. 2014. mCSM: predicting the effects of mutations in proteins using graph-based signatures. *Bioinformatics.* 30:335–342.

41. Guerois, R., J. E. Nielsen, and L. Serrano. 2002. Predicting changes in the stability of proteins and protein complexes: a study of more than 1000 mutations. *J. Mol. Biol.* 320:369–387.

42. Kastritis, P. L., and A. M. Bonvin. 2013. Molecular origins of binding affinity: seeking the Archimedean point. *Curr. Opin. Struct. Biol.* 23:868–877.

43. Cunningham, B. C., P. Jhurani, …, J. A. Wells. 1989. Receptor and antibody epitopes in human growth hormone identified by homolog-scanning mutagenesis. *Science.* 243:1330–1336.

44. Petkovic, V., M. C. Miletta, …, P. E. Mullis. 2013. Short stature in two siblings heterozygous for a novel bioinactive GH mutant (GH-P59S) suggesting that the mutant also affects secretion of the wild-type GH. *Eur. J. Endocrinol.* 168:K35–K43.

45. Yang, N., J. F. Langenheim, …, S. J. Frank. 2008. Activation of growth hormone receptors by growth hormone and growth hormone antagonist dimers: insights into receptor triggering. *Mol. Endocrinol.* 22:978–988.

46. Filikov, A. V., R. J. Hayes, …, B. I. Dahiyat. 2002. Computational stabilization of human growth hormone. *Protein Sci.* 11:1452–1461.

47. Clackson, T., and J. A. Wells. 1995. A hot spot of binding energy in a hormone-receptor interface. *Science.* 267:383–386.

48. Cunningham, B. C., and J. A. Wells. 1989. High-resolution epitope mapping of hGH-receptor interactions by alanine-scanning mutagenesis. *Science.* 244:1081–1085.

49. Wells, J. A. 1996. Binding in the growth hormone receptor complex. *Proc. Natl. Acad. Sci. USA.* 93:1–6.

50. Fernandes-Alnemri, T., J. Wu, …, E. S. Alnemri. 2007. The pyroptosome: a supramolecular assembly of ASC dimers mediating inflammatory cell death via caspase-1 activation. *Cell Death Differ.* 14:1590–1604.

51. Schroder, K., and J. Tschopp. 2010. The inflammasomes. *Cell.* 140:821–832.

52. Sahillioglu, A. C., F. Sumbul, …, T. Haliloglu. 2014. Structural and dynamics aspects of ASC speck assembly. *Structure.* 22:1722–1734.

53. Lu, A., V. G. Magupalli, …, E. H. Egelman. 2014. Unified polymerization mechanism for the assembly of ASC-dependent inflammasomes. *Cell.* 156:1193–1206.

54. Liepinsh, E., R. Barbals, …, G. Otting. 2003. The death-domain fold of the ASC PYRIN domain, presenting a basis for PYRIN/PYRIN recognition. *J. Mol. Biol.* 332:1155–1163.

55. Vajjhala, P. R., R. E. Mirams, and J. M. Hill. 2012. Multiple binding sites on the pyrin domain of ASC protein allow self-association and interaction with NLRP3 protein. *J. Biol. Chem.* 287:41732–41743.

56. Cai, X., J. Chen, …, Z. J. Chen. 2014. Prion-like polymerization underlies signal transduction in antiviral immune defense and inflammasome activation. *Cell.* 156:1207–1222.

57. Hershey, J. R., and P. A. Olsen. 2007. Approximating the Kullback Leibler divergence between Gaussian mixture models. *Proc. IEEE Int. Conf. Acoust. Speech Signal Process.* 4:317–320.

58. Bakan, A., and I. Bahar. 2009. The intrinsic dynamics of enzymes plays a dominant role in determining the structural changes induced upon inhibitor binding. *Proc. Natl. Acad. Sci. USA.* 106:14349–14354.

59. Liu, L., A. M. Gronenborn, and I. Bahar. 2012. Longer simulations sample larger subspaces of conformations while maintaining robust mechanisms of motion. *Proteins.* 80:616–625.

60. Shannon, P., A. Markiel, …, T. Ideker. 2003. Cytoscape: a software environment for integrated models of biomolecular interaction networks. *Genome Res.* 13:2498–2504.